ASEE AMERICAN SOCIETY FOR ENGINEERING EDUCATION

Paper ID #40374

Flow Changes of Vestibular System due to Changes in Volume and Ellipticity

Mr. Vincent Rodney Sheeler, Ohio Northern University

Vincent is a mechanical engineering student from Ohio Northern University. His interests in research are in topics of fluid dynamics, heat transfer, computational fluid dynamics, and thermodynamics.

Ms. Lacey Lynn Wernoch, Ohio Northern University

Lacey Wernoch is a senior mechanical engineering student at Ohio Northern University with a bioengineering concentration and a Spanish minor. In her professional future, she would like to work with biomechanics, biomaterials, or medical instruments.

Dr. Jed E. Marquart P.E., Ohio Northern University

Jed Marquart received his B.S.M.E. from Ohio Northern University, and his M.S. and Ph.D. in aerospace engineering from the University of Dayton. His 11 years in industry were spent primarily working for the U.S. Air Force in the areas of computational fl

Dr. Hui Shen, Ohio Northern University

Dr. Hui Shen is a professor at Ohio Northern University. Her research interests lie in mechanical behavior of materials, biomaterials, and biomechanics.

Flow Effects in Vestibular System

Vincent R. Sheeler
Department of Mechanical Engineering
Ohio Northern University
Ada, OH 45810, USA
Email: v-sheeler@onu.edu

Lacey L. Wernoch
Department of Mechanical Engineering
Ohio Northern University
Ada, OH 45810, USA
Email: l-wernoch@onu.edu

Jed E. Marquart
Department of Mechanical Engineering
Ohio Northern University
Ada, OH 45810, USA
Email: j-marquart@onu.edu

Hui Shen
Department of Mechanical Engineering
Ohio Northern University
Ada, OH 45810, USA
Email: h-shen@onu.edu

Proceedings of the 2023 ASEE North Central Section Conference

Abstract
Motion sickness is a very common condition shared among human beings. The generally accepted explanation for motion sickness is a disconnect between the motion the brain is expecting and the experienced motion. Many studies have been performed to investigate the external inputs and internal factors related to an individual's susceptibility of motion. There is no general agreement on the definitive cause of motion sickness. It is our great interest to explore why some individuals are more sensitive to motion. The vestibular system located in the human inner ear is important in sensing motion and maintaining balance of the body. It is difficult to research pressure differences experimentally in the ear because of how small the vestibules are and the inadequacies of current measuring tools. Computational fluid dynamics was therefore used to model the vestibules to observe fluid movement and pressure distributions in the middle ear. Flow differences around varied structures could explain what causes some humans to be sensitive to mechanical stresses and help explain the experience of motion sickness. The superior vestibule was modeled and analyzed as the head is rapidly turned. It was found that computational fluid dynamics can be utilized to observe the desired flow characteristics of the system.

Nomenclature

dt	=	time step (sec)
CFL	=	*Courant-Friedrichs-Lewy Number*
ρ	=	air density (kg/m^3)
u	=	x-component (cm)
v	=	y-component (cm)
w	=	z-component (cm)
U-velocity	=	fluid velocity in the x- direction (cm/s)

Introduction
The vestibular system is responsible for spatial orientation, maintenance of balance, and stabilizing vision [1]. The middle ear (ME) contains three semicircular canals, which sense head rotations and angular accelerations by external forces and maintain dynamic equilibrium. Each canal is oriented differently: horizontally, superiorly, and posteriorly. Within each of the semicircular canals are an ampulla and a cupula as shown in Figure 1 [2].

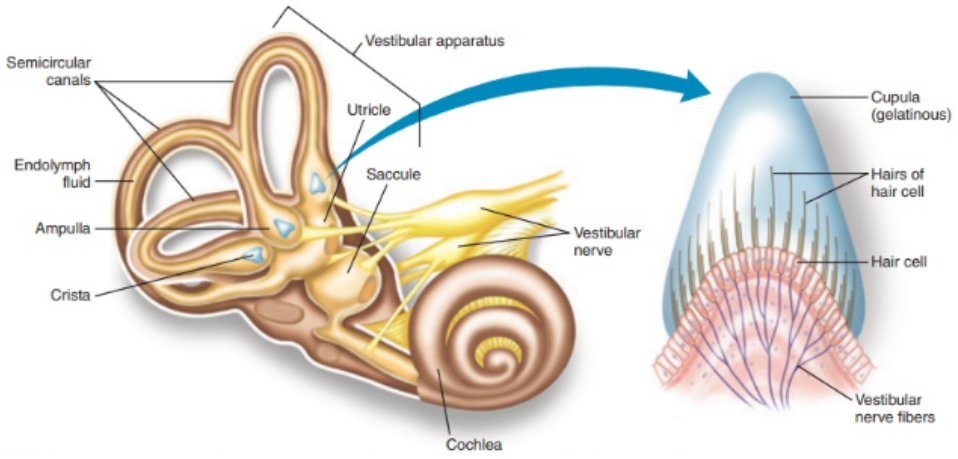

Figure 1: Model of middle ear semicircular canals, ampulla, cupula, and containing features [3].

The ampulla is the bulbous expansion that is innervated by hair cells, the primary receptor cells for transducing movement to the brain, and crista, which sense angular acceleration. The cupula is a gelatinous structure at the end of the semicircular canal that provides spatial orientation [4]. When the head is turned, the fluid in the canals moves, the cupula is distorted, and the hair cell bundles in the crista are moved. The nerves in the hair cell bundles send signals to the brain that the body is moving, and the body should orient in response [2]. Together the ampulla and the cupula provide stable orientation and balance within people. By computationally modeling the fluid filled semicircular canals the importance of the pressure distribution and fluid flow on the ampulla can be understood.

Models

Vestibule Models

To better understand the structural impact of the superior vestibule on fluid movement the ellipticity and volume of the vestibule system were varied for a total of five models. In all models, the vestibular system was idealized to assume the semicircular canal as a toroid shape and the ampulla as a bulb. The base model was dimensioned according to research to accurately mimic the vestibule system as measured. The geometry was constructed using splines to maintain a circular tube all the way around the toroid. The diameter of the tube was chosen to be 0.4mm, the height of the structure was chosen to be 6.9mm, and the width of the structure was chosen to be 7.24mm respectively [1]. To create the V+1 model, the base model was scaled to 120%. To create the V-1 model, the base model was scaled to 80%. To create the E+1 model, the height of the splines used to construct the tubes was scaled to 120% of the base. Similarly, the E-1 model was constructed by scaling the height of the splines to 80% of the base model. This leaves the ellipticity variations with the same size cupula as the base model. Figures 2, 3, 4, 5, and 6 show the following model variations. Additionally, the model dimension variations shown in Figures 2-6 are summarized in Table 1.

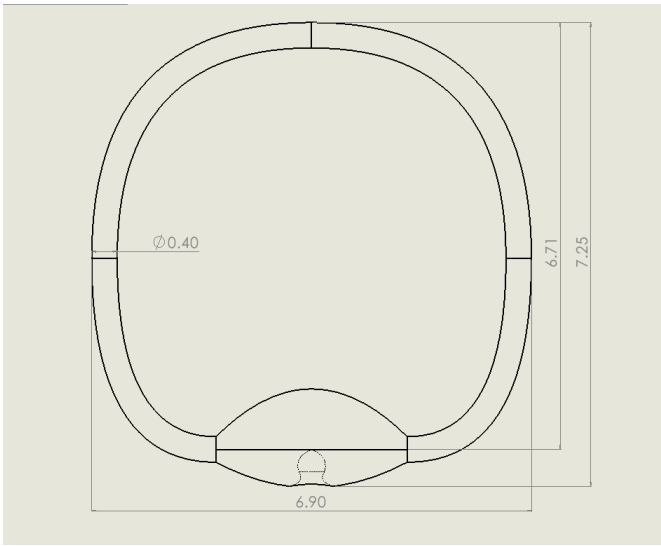

Figure 2: Dimensioned base model.

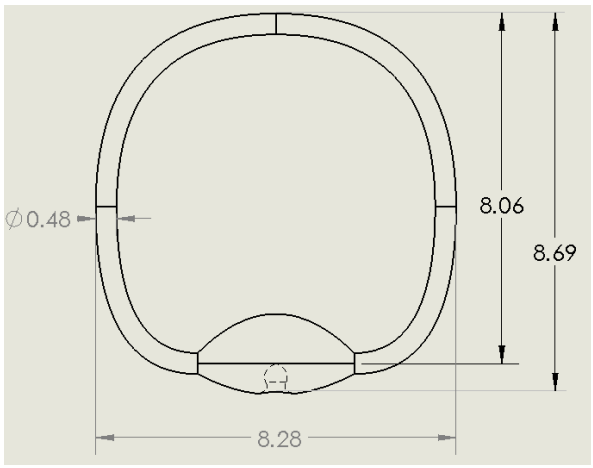

Figure 3: V+1 dimensioned model.

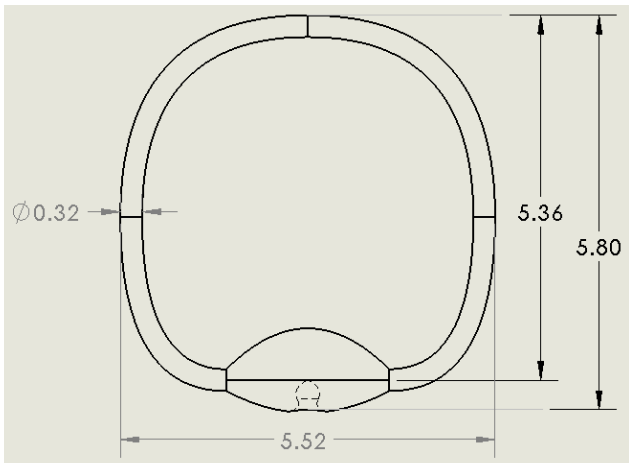

Figure 4: V-1 dimensioned model.

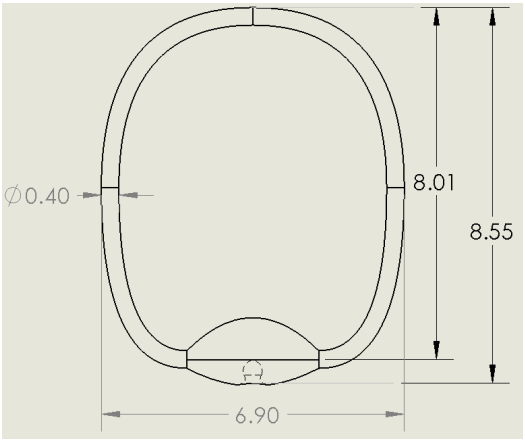

Figure 5: E+1 dimensioned model.

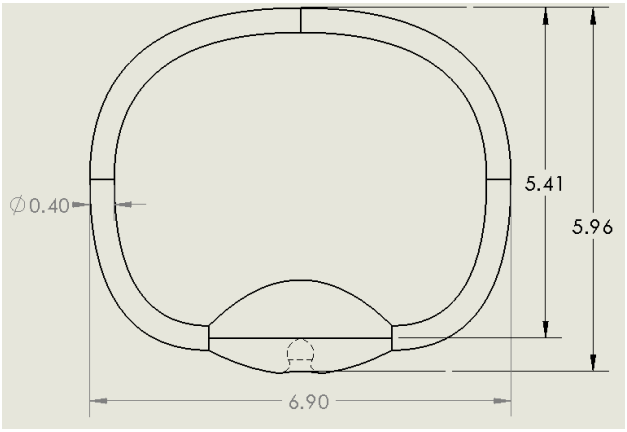

Figure 6: E-1 dimensioned model.

Table 1: Model dimension variations

Model	**Scaling Factor**	**Tube Diameter (mm)**	**Overall Width (mm)**	**Ampulla Height (mm)**	**Overall Height (mm)**	**Total Volume (mm^3)**
Base	-	0.40	6.90	6.71	7.25	4.90
V+1	120% of volume	0.48	8.28	8.06	8.69	8.47
V-1	80% of volume	0.32	5.52	5.36	5.8	2.51
E+1	120% of spline height	0.40	6.90	8.01	8.55	5.17
E-1	80% of spline height	0.40	6.90	5.41	5.96	4.63

Because the modeling software and flow solvers used do not support semi-solid bodies, the cupula model was made as a solid cutout to act as a flow barrier. Figures 7 and 8 show the overall dimensions of the ampulla [1].

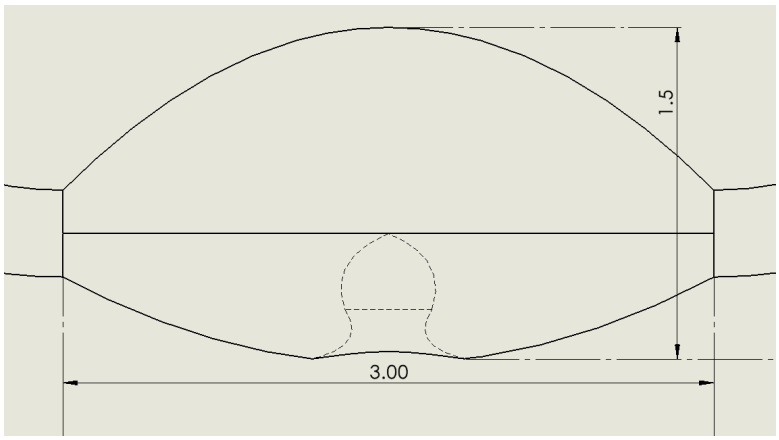

Figure 7: Ampulla Front View

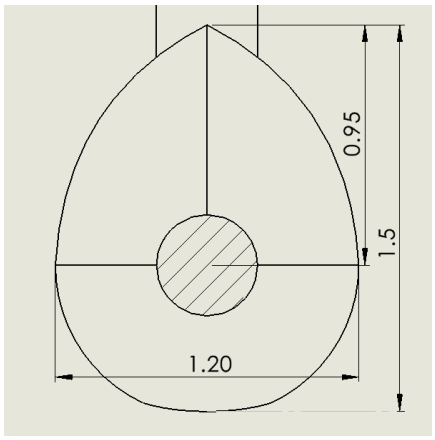

Figure 8: Ampulla Side View

The dimensions of the ampulla were idealized to 3mm across and 1.5mm tall, the vestibular tubes are centered with the ampulla. The cupula was modeled to be 0.575mm tall, and 0.5mm at its widest. The profile of the cupula was cut from the ampulla in a circle to create a barrier to flow. Figure 9 shows a detailed drawing of the cupula used for geometry.

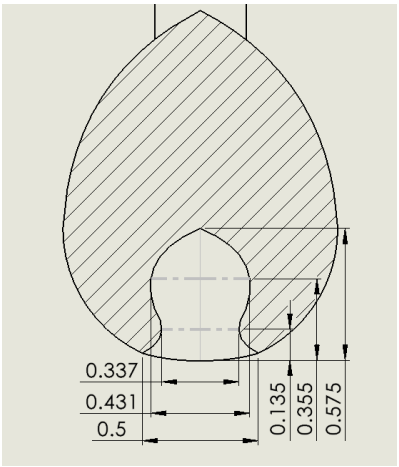

Figure 9: Cupula Dimensions

Grid Modeling

Each model's grid was created in a standard way, creating domains, creating blocks, and then generating layers of anisotropic tetrahedral from the boundary grid. An angular velocity of 500rpm was chosen for simulation to emphasize flow effects. To allow for examining each model as time-dependent, a dt was chosen ahead to have a CFL close to 1.

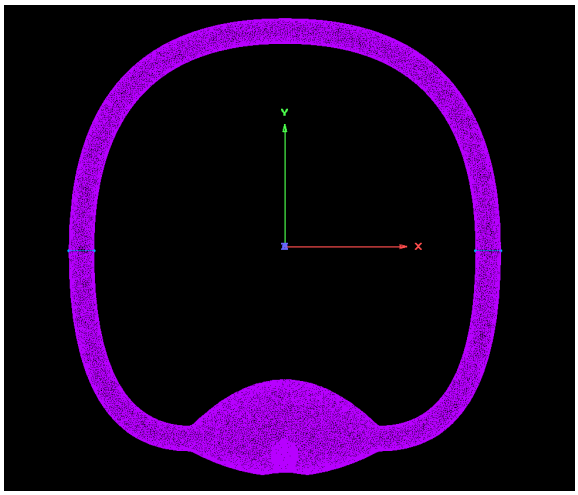

Figure 10: Base Model Domains

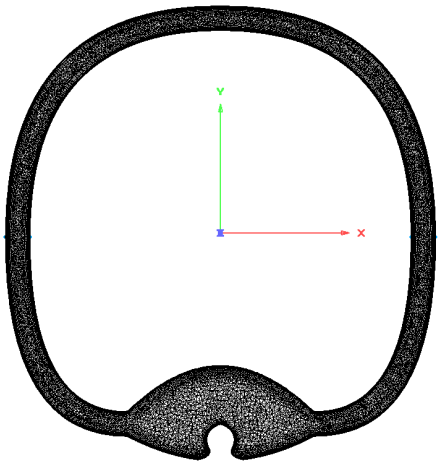

Figure 11: Base Model Volume Mesh

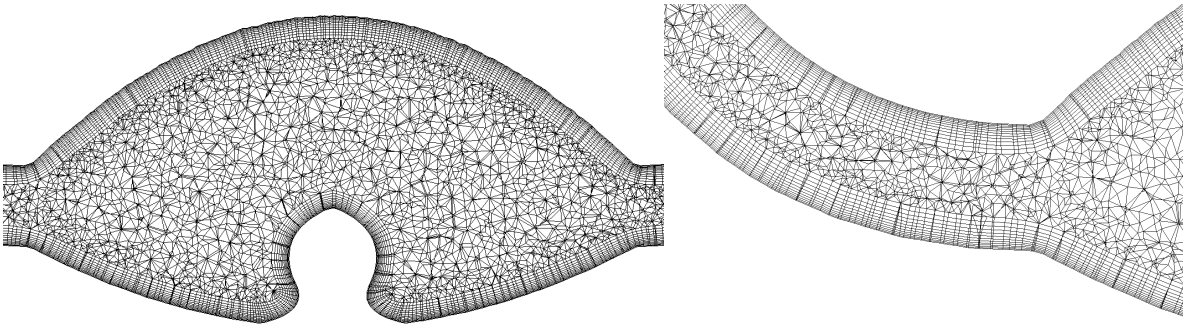

Figure 12: Local Volume Mesh Visualization

The exact cell counts, and anisotropic tetrahedral settings vary between models to ensure they each reach at least the recommended 93% grid quality, as calculated, and reported by the flow solver, Cobalt. General no slip walls were used for the boundary conditions for this project. The exact grid settings and grid information can be found in Table 2.

Table 2: Model Grid Conditions

Model	Total Points	Total Cells	Grid Quality (%)	dt (sec)	Initial Δ	Layers	Growth Rate	Decay
Base	336,505	798,039	94.72	2.29E-08	0.0003	12	1.15	0.7
V+1	330,425	752,267	94.46	2.80E-08	0.0005	12	1.15	0.7
V-1	341,327	807,473	94.90	2.14E-08	0.0003	12	1.15	0.7
E+1	370,579	876,819	94.85	2.27E-08	0.0003	12	1.15	0.7
E-1	303,194	695,519	94.36	2.36E-08	0.0003	12	1.20	0.7

The goal of the study is to observe the flow of endolymph fluid through the vestibular system for a rapid head rotation. The primary results to focus on will be the fluid velocity and pressure across the vestibular system in these simulations. The flow solver also does not support modeling liquids, so an ideal gas, air, was used. All models used the same reference conditions for their

simulations, air at Mach 0.005, standard temperature, and standard pressure. The rapid turn of the head was simulated by setting a turn of the vestibular model around an offset axis of rotation (AR), set parallel to the y-axis 87.5 mm in the z-direction as shown in Figure 10. The average human head width varies from 152.4-178.0 mm wide; a head width of 175 mm was used for all models [2]. By distancing the AR half of the head's width away from the vestibular model, 87.5mm, the rotation axis was aligned to the center as seen in Figure 13.

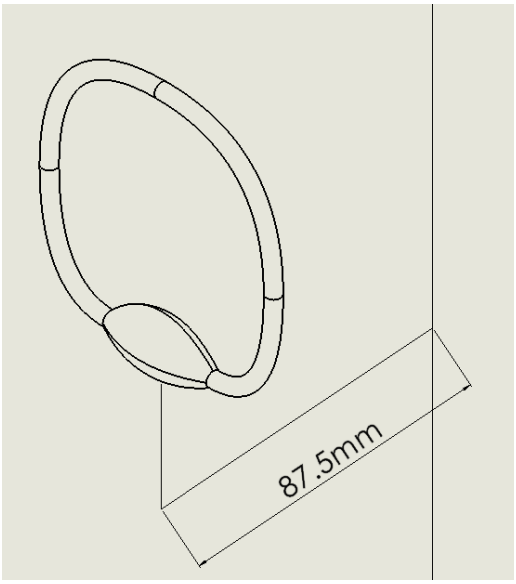

Figure 13: Axis of Rotation Visualization (Not to scale)

Mathematical Modeling

The flow solver used, *Cobalt*, is a commercial, implicit, hybrid-grid Euler/Navier-Stokes solver based on a cell-centered finite volume approach. Viscous fluid flow is governed by the Navier-Stokes equations. In integral form, these equations are given by Equation 1:

$$\frac{\partial}{\partial t}\iiint_V \boldsymbol{q}\,dV + \iint_S (\boldsymbol{f}\hat{i} + \boldsymbol{g}\hat{j} + \boldsymbol{h}\hat{k})\cdot \hat{n}\,dS = \iint_S (\boldsymbol{r}\hat{i} + \boldsymbol{s}\hat{j} + \boldsymbol{t}\hat{k})\cdot \hat{n}\,dS \tag{1}$$

where:

$$\boldsymbol{q} = \begin{bmatrix} \rho \\ \rho u \\ \rho v \\ \rho w \\ \rho E \end{bmatrix} \quad \boldsymbol{f} = \begin{bmatrix} \rho u \\ \rho u^2 + p \\ \rho uv \\ \rho uw \\ u(\rho E + p) \end{bmatrix} \quad \boldsymbol{g} = \begin{bmatrix} \rho v \\ \rho uv \\ \rho v^2 + p \\ \rho vw \\ v(\rho E + p) \end{bmatrix} \quad \boldsymbol{h} = \begin{bmatrix} \rho w \\ \rho uw \\ \rho vw \\ \rho w^2 + p \\ w(\rho E + p) \end{bmatrix}$$

and:

$$\boldsymbol{r} = \begin{bmatrix} 0 \\ \tau_{xx} \\ \tau_{xy} \\ \tau_{xz} \\ u\tau_{xx} + v\tau_{xy} + w\tau_{xz} + kT_x \end{bmatrix} \quad \boldsymbol{s} = \begin{bmatrix} 0 \\ \tau_{yx} \\ \tau_{yy} \\ \tau_{yz} \\ u\tau_{yx} + v\tau_{yy} + w\tau_{yz} + kT_y \end{bmatrix} \quad \boldsymbol{t} = \begin{bmatrix} 0 \\ \tau_{zx} \\ \tau_{zy} \\ \tau_{zz} \\ u\tau_{zx} + v\tau_{zy} + w\tau_{zz} + kT_z \end{bmatrix}$$

Results and Discussion

To find a solution, the model was run in *Cobalt* and then processed in *FieldView*. Endolymph fluid has similar properties to water, but *Cobalt* is limited to ideal gas as its only fluid. Air is set as the ideal gas to be used by entering the properties of air, but other ideal gases could have been modeled similarly. Though magnitudes of the results may differ, the behavior of the fluid is most important to understand as the main point of interest for this study is the differences in flow near the cupula. For comparing models, a line was drawn connecting the centers of the inlet and outlet. *FieldView* then places points on the line according to the volume mesh. Because of the idealized geometry, this places the line nearly tangent to the tip of the cupula. As a result, plots show the flow entering and exiting the boundary layer surrounding the cupula. Figure 14 shows the reference line used for the base model to compare varied models' behavior along, with the left-hand side being the beginning.

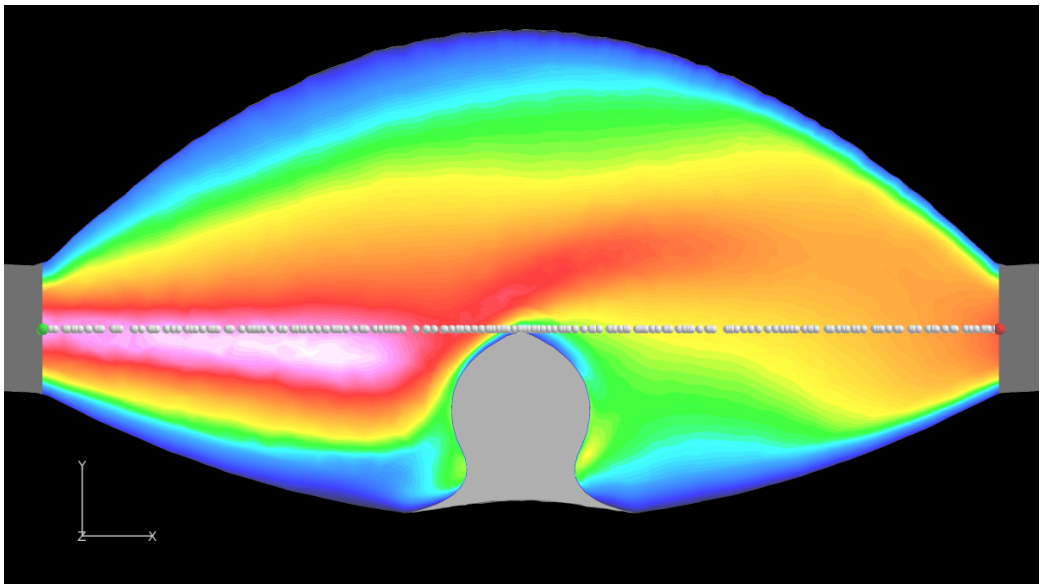

Figure 14: Plot line visualization

In terms of U-velocity, changes in ellipticity resulted in minor differences in velocity, while the changes in volume resulted in greater differences. Table 3 compares models' U-velocity to the base model at the inlet and outlet respectively. The changes in U-velocity correlate to each model's change in volume. Models V+1 and E+1 each have higher total volumes and lower velocities while V-1 and E-1 have lower volumes and higher velocities.

Table 3: U-Velocity Model Comparisons

Change in U-Velocity		
Model	**Inlet**	**Outlet**
V+1	-34.97%	-15.75%
V-1	+17.70%	+19.04%
E+1	-3.05%	-2.24%
E-1	+5.39%	+2.19%

As mentioned before, the plotted path enters the boundary layer near the cupula. As a result, U-velocities of each model rapidly drop between the fluid entering the ampulla at near 45% and fully exiting the boundary layer around 55%. This remains consistent for all models and U-velocity plots as shown in Figure 15 below.

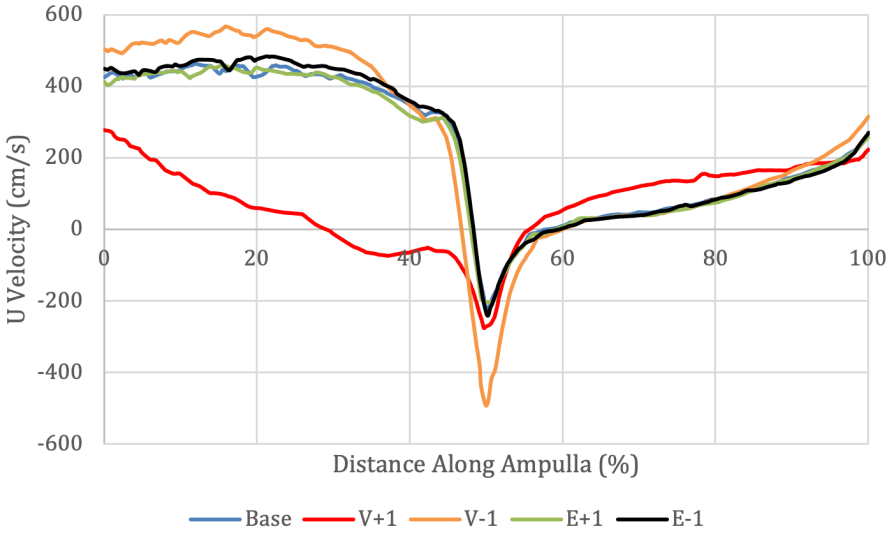

Figure 15: U-Velocity Plot

For all models, gage pressure across the ampulla does not significantly change. Base, E+1, and E-1 models all have the same size ampulla. Thus, their changes in pressure are directly due to the ellipticity change. The V-1 model shows much larger gage pressures compared to all other models. This is most likely due to the smaller inlet and exit areas. This overall demonstrates that significant changes in pressure can occur from ellipticity. Table 4 shows the models' impact on pressure changes in terms of percent change.

Table 4: Models' Effects on Pressure

Model	Change in Volume	Tube Diameter (mm)	Average Gage Pressure (kPa)	Change in Gage Pressure
Base	-	0.4	2.249	-
V+1	72.86	0.48	2.160	-3.96%
V-1	-48.78	0.32	4.576	103.47%
E+1	5.51	0.4	2.561	13.87%
E-1	-5.51	0.4	1.940	-13.74%

As seen in Figure 16, gage pressures of each model did not change significantly from their initial gage pressure over the distance of the ampulla.

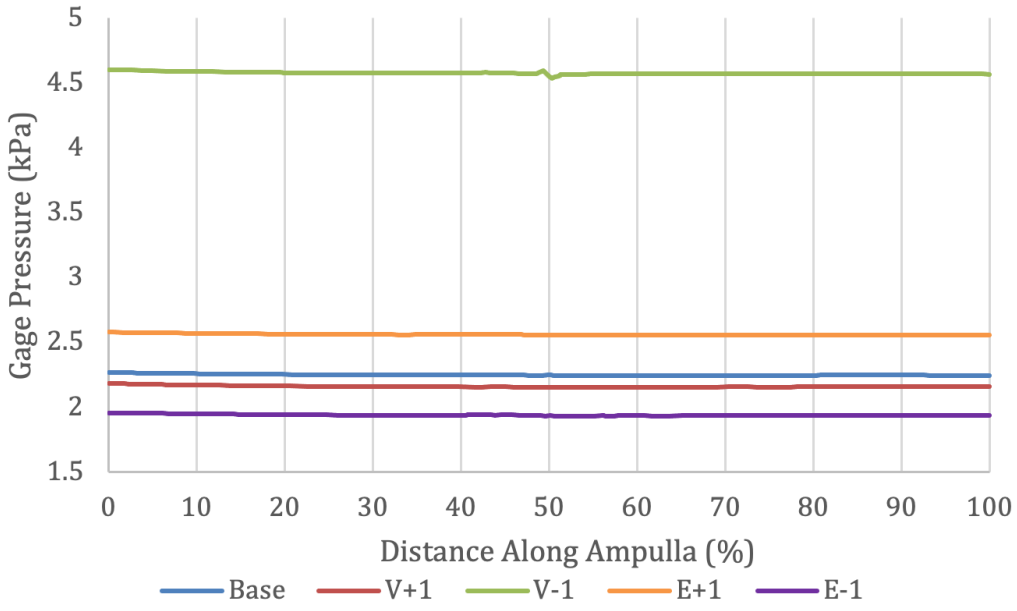

Figure 16: Gage pressure along ampulla plot

The pressure on the entry side of the model remains higher than the pressure on the exit side to continue moving fluid through the system. Concentrated pressure in the entry tube has a larger net force that accelerates fluid movement after the cupula. By solving the equations of motion, regions of higher velocity will have lower pressure and regions of lower velocity have higher pressure. Though both V+1 and E-1 have a low pressure in the ampulla, V+1 has a much higher concentration of pressure in the entry tube than E-1 so that V+1 results in a greater U-velocity. E+1 and E-1 have similar pressure distributions to the base, so have similar U-velocities throughout the ampulla as shown in Figure 15. V-1 has a much higher overall pressure than the other models but ends up behaving more like the base's U-velocity after the cupula because the pressure concentration in the entry tube is so like the base's. The effects of U-velocity because of pressure distribution in the models can be seen in Figures 17- 26.

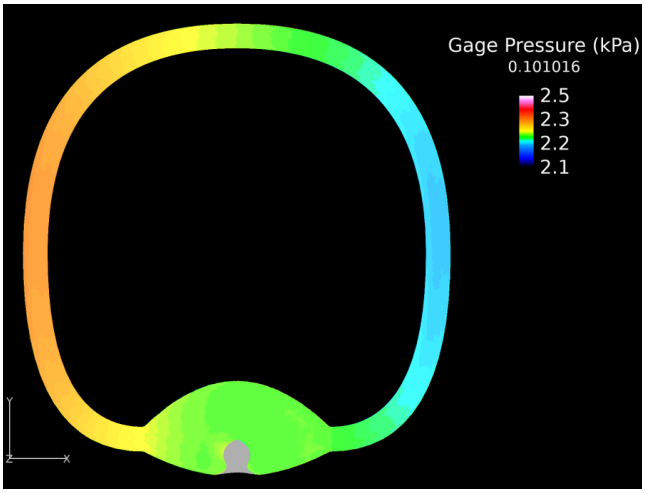

Figure 17: Base pressure distribution

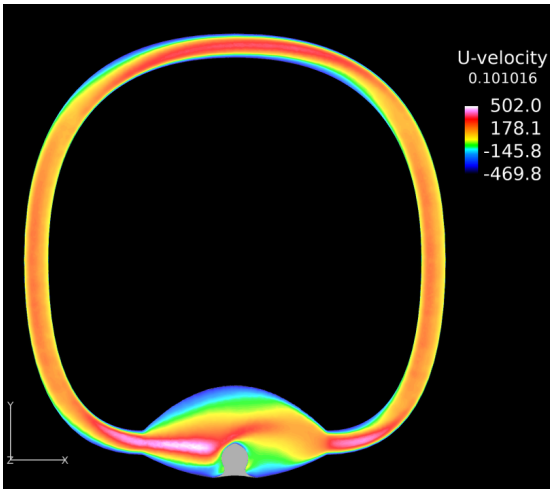

Figure 18: Base U-velocity

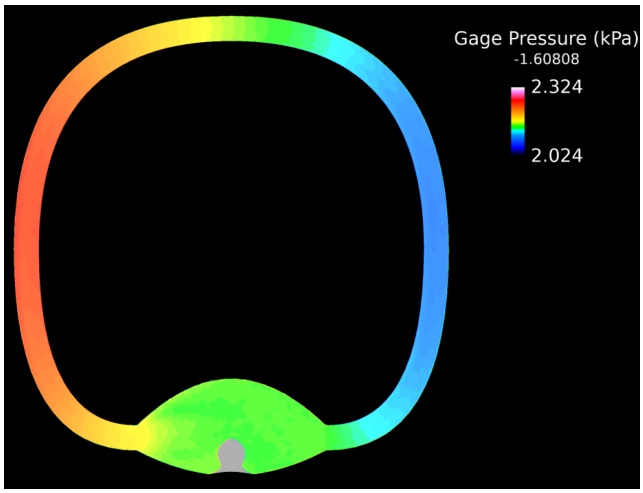

Figure 19: V+1 pressure distribution.

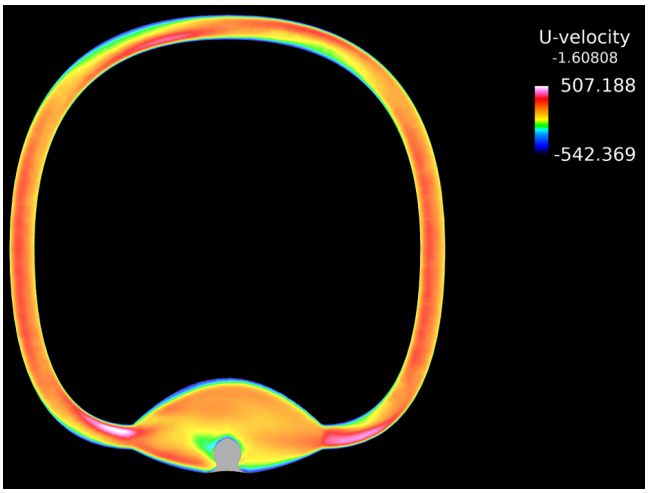

Figure 20: V+1 U-velocity.

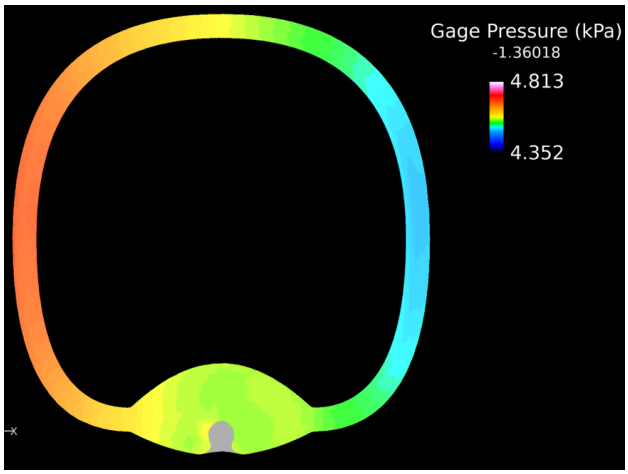

Figure 21: V-1 pressure distribution.

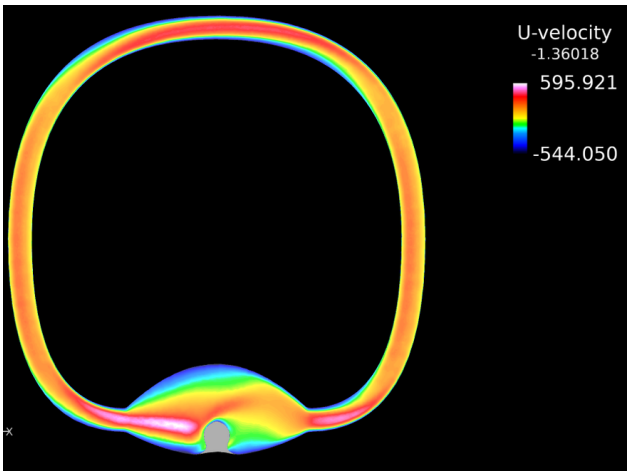

Figure 22: V-1 U-velocity.

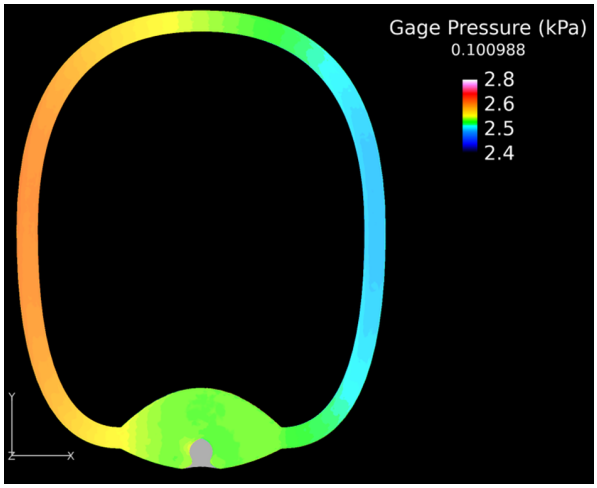

Figure 23: E+1 pressure distribution.

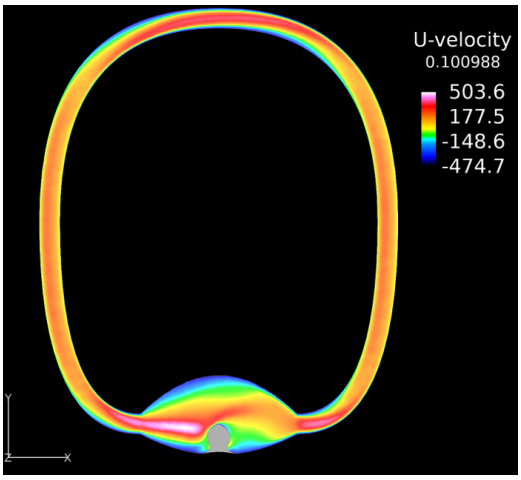

Figure 24: E+1 U-velocity.

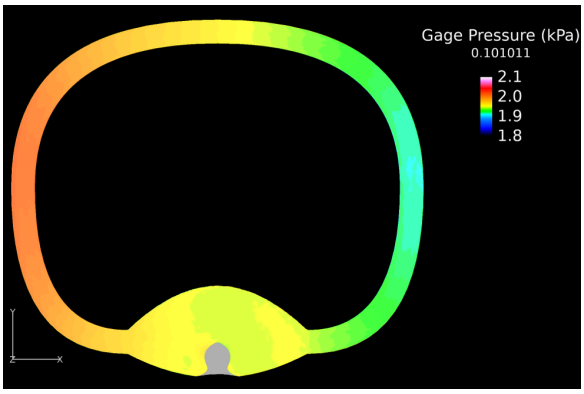

Figure 25: E-1 pressure distribution.

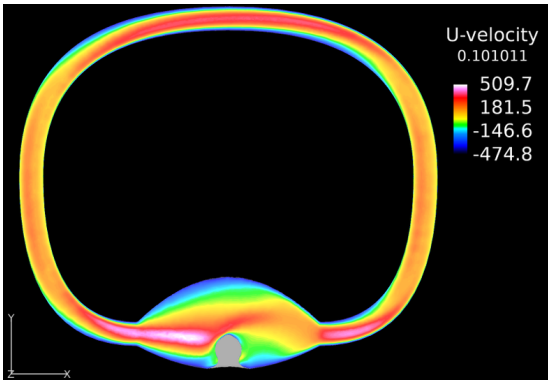

Figure 26: E-1 U-velocity.

In addition to U-velocity there is also V- and W-velocity that contribute to fluid movement. V- and W-velocity do not have significant influences on their own but provide influential magnitude altogether. U-velocity is the dominant factor in velocity magnitude, so was chosen to be focused on. By understanding the behavior of U-velocity, velocity magnitude was able to be predicted to follow the same behavior. Like U-velocity, volume continues to have the greatest influence on velocity magnitude as shown in Table 5.

Table 5: Change in Velocity Magnitude

Change in Velocity Magnitude		
Model	**Inlet**	**Outlet**
V+1	-31.32%	-14.63%
V-1	+17.56%	+18.44%
E+1	-2.98%	-2.41%
E-1	+5.02%	+2.44%

Velocity magnitude varies before reaching the cupula but reaches similar values at the exit of the ampulla. The pressure differences previously shown explain the velocity magnitude differences shown in Figure 27.

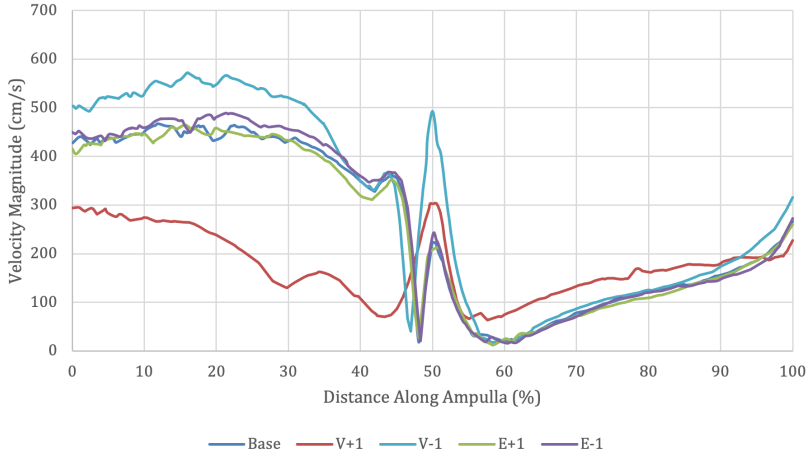

Figure 27: Velocity magnitude plot

Conclusions and Recommendations

In this paper, the computational fluid dynamics method was used to study the effect of the geometry parameters, including ellipticity and volume of the semicircular canal, on the fluid movement and pressure distributions in the vestibular system. The velocity results show that volume has the greatest effect on fluid movement and pressure distributions in the vestibular system. As the fluid force moves the cupula and the hairs on it, signals of movement are sent to the brain that outlast the actual movement of the vestibular system. Dually, the fluid moves at an uneven rate within the tubes that unevenly stimulate the nerve hairs. Both the outlasting fluid effects, and uneven stimulation could create an unsteady sense of balance in a person. Therefore, it can be concluded that the difference in the geometry of an individual's vestibule could lead to different responses to motion under the same motion input. This result might explain why some individuals are more sensitive to motion than others.

As aforementioned, the results were analyzed with air instead of endolymph fluid. For future work, the model could be scaled to reflect the liquid's properties like endolymph fluid to obtain more accurate results. An experiment comparing varied vestibular system volumes and movement sensations would help draw conclusions on fluid movement and experiences of motion sickness.

Acknowledgments

We would like to thank the IT department at Ohio Northern University for the technical support.

References

[1] I. S. Curthoys, C. H. Markham, and E. J. Curthoys, "Semicircular duct and ampulla dimensions in cat, guinea pig and man," *Journal of Morphology*, vol. 151, no. 1, pp. 17–34, 1977.
[2] "What is the average size of the human head?," *Reference*, 27-May-2020. [Online]. Available: https://www.reference.com/science-technology/average-size-human-head-62364d028e431bf3.
[3] *Cobalt Manual, Version 8*, Cobalt Solutions, LLC, Dayton, OH, 2018.